GEMINI
8-M Telescopes
Project

RPT-O-G0034
Rev 2

Distortion of the Primary Mirror Due to Temperature and CTE Nonuniformity

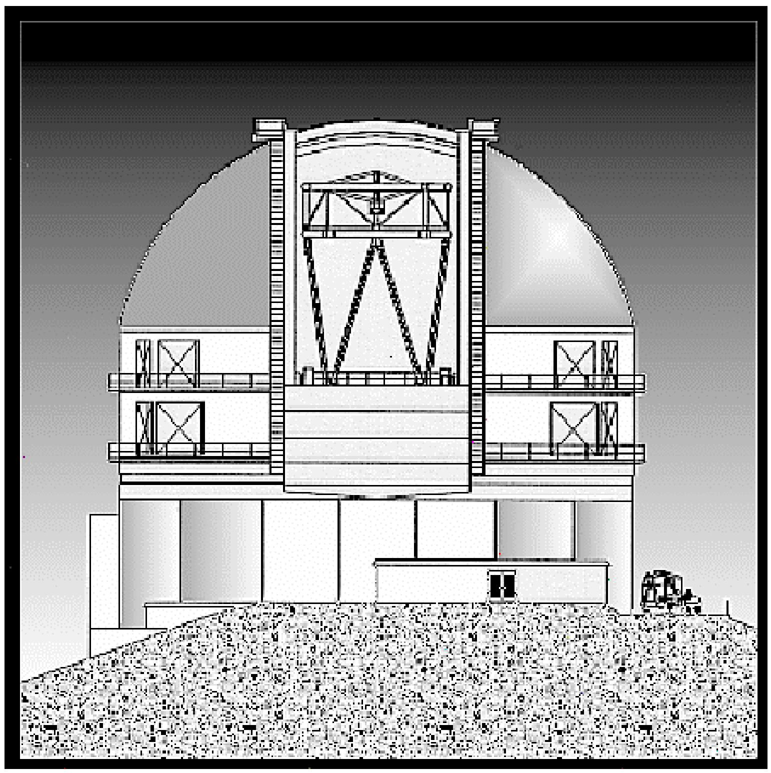

Myung Cho
Opto-Structural Engineer

Eric Hansen
Opto-Mechanical Engineer

August 11, 1995

GEMINI PROJECT OFFICE   950 N. Cherry Ave.   Tucson, Arizona 85719
Phone: (520) 318-8545   Fax: (520) 318-8590

Summary

This report outlines the methods and results of modeling used to predict the distortion of the primary mirror due to temperature gradients and coefficient of thermal expansion variations within the primary mirror. Finite element modeling was used simulate various temperature distributions and to find the optical surface deformations that were induced. Coefficient of thermal expansion (CTE) data from the mirror fabricator was used to estimate the expected range of CTE for boules used in the primary mirror. A distribution of boules within the primary mirror that minimized the thermally induced deformations was used for modeling. The optical surface error and its effect on image quality were then found both before and after active optics correction. Due to the low CTE of the ULE*TM* primary mirror, the magnitude of these deformations are low even with large temperature gradients. In addition, the smooth shape and slow change rate typical of thermally induced errors in a solid mirror substrate allows these already small deformations to be corrected to negligible levels using active optics.

Table of Contents

Section 1
INTRODUCTION

1.1 Purpose of Analyses

In order to predict the optical surface errors caused by thermal gradients and temperature changes within the primary mirror, temperature and CTE distributions were modeled using finite element methods. The errors analyzed fall into two broad categories. The first deals with errors caused by nonuniform temperature distributions. Many experiments *(Ref 1,2)* have shown the difficulty of obtaining isothermal conditions in glass mirror blanks even under laboratory conditions. Because ULE has a low but nonzero coefficient of thermal expansion, gradients through the thickness of the blank can produce localized bending, leading to wavefront aberrations.

The second category deals with the surface errors that are caused by nonuniform CTE. The CTE of individual boules that make up the primary mirror vary slightly from one to another. Because of these variations, a change in temperature, such as between the optics shop and observatory, can cause bending of the mirror. Each boule is individually characterized by measurement of CTE at the fabricator in both radial and axial directions. By distributing the boules in the primary mirror with regard to their CTE, the effects of their variations can be minimized. An optimization algorithm to place each of boules (hexes) in the GEMINI primary mirror blanks was developed. This optimization ensures that the locations of the individual hexes in the mirror blank minimize the optical surface distortion due to the CTE variations The Japanese National Large Telescope (JNLT) developed a method to optimize boule distributions *(Ref 4)*.

1.2 Description of Model

Figure 1 shows the finite element model used in this analysis. It consists of four layers of solid elements with 588 elements on each layer for a total thickness of 0.2 meters. The upper layer of nodes represent the optical surface and have a spherical radius of curvature of 28.8 meters. The inner and outer diameters are 1.2 and 8.0 meters.

1.2.1 Material Properties

The properties of ULE that were used in the model are summarized below.

Coefficient of Thermal Expansion	-40 PPB
CTE Maximum Variation	+/-15 PPB
Density	2.205 gm/cm3
Poisson's Ratio	0.17
Elastic Modulus	67.6 GPa

1.2.2 Temperature Distributions

Six temperature distributions were analyzed in this study. Each distribution has a minimum to maximum deviation of one degree Celsius. The temperatures were input using mathematical functions that provided distributions that simulate possible operational conditions. The individual cases are described below.

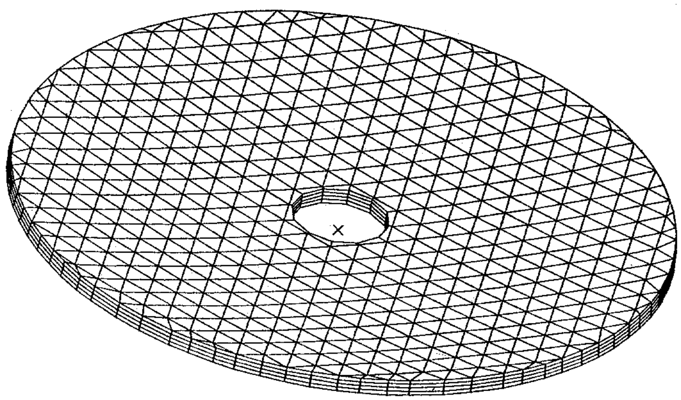

Figure 1 Finite Element Model

Case I provides a linear gradient through the thickness of the mirror, from 0.0 degrees at the rear surface to 1.0 degrees at the optical surface. This models the gradient that may be produced by the proposed thermal control system, from a uniform heating or cooling of the rear surface. This case also provides deformation results that can quickly be checked against closed form solutions for solid disks with temperature gradients

Case II uses a linear gradient along the radius of the mirror, from 0.0 degrees at the inner diameter to 1.0 degrees at the outer diameter.

Case III models nonuniformities at the outer edge of the primary mirror. There are a number of possible causes for this edge effect. Because of interference with the air pressure support seals the radiation plate may not extend to the full outer and inner diameters of the mirror. This would cause a slight reduction in the rate of heat transfer at the edge of the mirror. In addition, modeling of the proposed surface heating concept has shown increased heating rates near the electrodes which are on the inner and outer diameters. The distribution was taken from the results of a finite element model and scaled for a 0.0 to 1.0 degree range. This model evaluated the effect of an air pressure seal limiting the view factor between radiation plate and primary.

Case IV provides a temperature distribution that was found to produce large surface deformations in a previous study *(Ref 3).* This case uses an astigmatic distribution over the front and rear surfaces with a range of +/- 0.5 degrees. The front and rear distributions are rotated 90 degrees with respect to each other. This yields a +0.5 temperature on the upper surface directly above a -0.5 temperature at the lower surface. The gradient through the thickness of the mirror is linear.

Case V models a random temperature distribution across the optical surface with a three sigma error of 1.0 degree. As was mentioned earlier, temperature uniformity in large glass blanks is difficult to achieve even under laboratory conditions. This case attempts to quantify the effects of temperature nonuniformity.

Case VI is a localized 1.0 degree temperature increase, placed on a single element. This simulates the temperature distribution from a localized heat source in the mirror cell.

1.2.3 CTE Distributions

This model used a distribution of boules within the primary mirror, that was based on the CTE measurements of the GEMINI primary mirror blank #1. The range of axial CTE gradient variation between boules was +/- 7 PPB, and the volumetric average radial CTE was +/- 4 PPB. These CTE measurements were based on actual Gemini Project boules fabricated and tested.

Case VII evaluates the result of uniform temperature change between polishing shop and mountain top environments. A one degree temperature difference was used for this case, the deformation can be scaled to represent expected temperature changes.

Section 2
ERROR BUDGET

2.1 General Error Budget

The *Gemini System Error Budget Plan, (Ref 5)* has established an allowable image degradation value for the primary mirror and its support system. It also establishes a maximum allowable value for any change in telescope plate scale, or effective focal length, (efl), change. The error budget, as it applies to the primary mirror, should be consulted for a complete detailing of the total system error budget and more in depth discussion of the errors that apply to the primary mirror.

2.2 Image Quality

The overall image degradation allowance for the thermal deformation of the primary mirror is .005 arcsecond increase in diameter for 50% encircled energy and .009 arcsecond for 85% encircled energy at a wavelength of 2.2 μm. The total image quality error budget allowance must be divided between several cases.

Seven cases were defined for evaluation. The summation of these cases must satisfy the requirements stated above.

2.3 Plate Scale

Requirements also exist for the change in telescope effective focal length (efl) caused by the primary mirror assembly. The total allowable change in plate scale is 100 parts per million (ppm). The allowance for the primary mirror is 50 parts per million, of which 45 ppm is allowed for primary mirror thermal errors. The allowance for thermal errors must be divided up amongst the various error cases. It is assumed that spherical curvature changes of the primary mirror will not be detected by the active optics wavefront sensor because the auto focus system will continually compensate. Therefore, it is assumed that the plate scale changes will not be corrected by active optics.

Section 3
ANALYSIS

3.1 Finite Element Analysis Methods

3.1.1 Finite Element Model

Deformations were calculated using I-DEAS finite element analysis, *(Ref 6)*. For these analyses a full model of the mirror was constructed. This was necessary due to the non-symmetric distribution of temperatures in some of the desired cases. The model consists of 2352 elements and 3060 nodes. It uses solid brick and wedge elements. A single temperature is used for each element. Deflections at each optical surface node due to each temperature distribution case were found assuming no restraint on the mirror. Each case was then analyzed to find the RMS deformation of the optical surface; this is referred to as raw data. Piston, tilt and focus were then removed and the RMS calculated again. At this point active correction was applied to the remaining deformations.

3.1.2 Active Optics Correction

Active optics correction is done by modeling the effect of 120 active actuator forces on the deformed mirror shape. The displacements over a uniform 64 by 64 grid are found as a result of active forces. Optimum actuator forces are calculated from a least squares minimization on the residual displacement errors. Active optics correction methods are described in more detail in *Active Optics Capability of the Gemini Primary Mirror System, (Ref 8)*.

The nodal positions used in this model do not correspond to the uniform grid. In order to find the deformed optical surface position at each grid point a 36 term zernike fit was used to characterize the optical surface. From this analytical description, the initial position of the surface at each grid point is found and then corrected using the best combination of active optics forces. Plots of mirror surface deformations before and after active optics correction are given in Section 4, Results.

3.2 Optical Analysis Methods

3.2.1 General Procedure

The mirror deformations generated by the finite element analyses were analyzed using the Code V optical analysis package *(Ref 7)*. Grid format interferogram files were generated from the deformation results of the finite element analyses. These files contain mirror surface deformations at each grid point. Prior to the analysis piston, tilt and focus were removed from the deformations. The amount of focus aberration removed was used in the calculation of the change in plate scale. The deformation grid file was applied to the primary mirror. Image quality and plate scale were then evaluated. The results are given in Section 4, Results.

3.2.2 Image Quality Analysis

Encircled energy was calculated using the diffraction based PSF option of Code V. The results were compared to the unaberrated telescope by quadrature subtraction. All image quality calculations were performed for the on axis field position. Many of the deformations analyzed are sufficiently small that calculation of the differences in encircled energy is difficult using the ray trace software. Scaling the deformations to a significant level and then scaling the quadrature difference back down by the same factor was found to improve the accuracy of the calculation. This method produces a conservative value for image degradation. The interferogram files were therefore scaled up to a surface error of 40 nm rms. The encircled energy was calculated for this surface and the quadrature difference was then reduced by the same scale factor.

3.2.3 Plate Scale Change

Plate scale changes were evaluated using the amount of focus aberration removed from the deformations of the finite element analysis. Paraxial ray trace analysis results show a plate scale change of one part in one million for a peak to valley change in focus aberration of the primary mirror of 159.9 nm.

Section 4
RESULTS

4.1 Deformations Summary

Table 4-1 summarizes the primary deformations before and after active optics correction for unit magnitude temperature distributions. Cases are described in section 1.

MIRROR SURFACE DEFORMATION

CASE NUMBER	RAW DATA RMS (NM)	P. T. F. REMOVED RMS (NM)	AFTER ACTIVE CORRECTION (NM)	MAXIMUM REQUIRED ACTIVE FORCE (N)
Case I	199.9	28.6	3.3	28
Case II	142.2	17.9	0.2	4
Case III	107.4	23.2	2.0	16
Case IV	288	238.1	4.3	59
Case V	6.8	4.3	0.3	9
Case VI	0.4	0.4	0.1	3
Case VII	23	4	0.35	1.9

Table 4-1 Thermal Deformations Summary

4.2 Effect on Image Quality and Plate Scale

Table 4-2 summarizes the effects on image quality degradation for all of the deformations after active correction as well as plate scale change. The values shown here are the increase in size of 50 and 85 percent encircled energy diameters.

CASE NUMBER	50% ENCIRCLED ENERGY (AS)	85% ENCIRCLED ENERGY (AS)	PLATE SCALE CHANGE PPM
Case I	3.64E-4	1.91E-3	4.64
Case II	2.65E-4	3.08E-3	3.41
Case III	2.86E-4	1.50E-3	2.42
Case IV	3.84E-4	5.01E-3	-1.65E-2
Case V	8.7E-5	4.61E-4	-1.4E-2
Case VI	3.0E-6	1.80E-5	1E-3
Case VII	8.0E-5	3.5E-4	1.75
RSS Total	6.68E-4	6.39E-3	6.49

Table 4-2 Image Quality Summary

4.3 Surface Contour Maps

Figures 2 through 8 show primary mirror surface contour maps for each analysis case both before and after active optics correction as described in Section 3, Analysis.

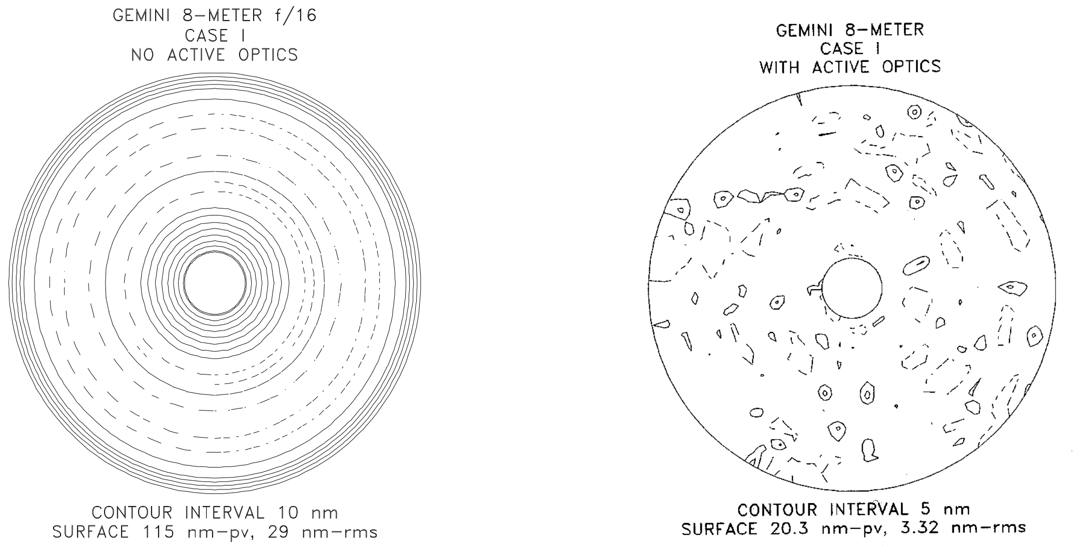

Figure 2. Case I before and after active correction, note the contour interval is 2 times smaller on the right.

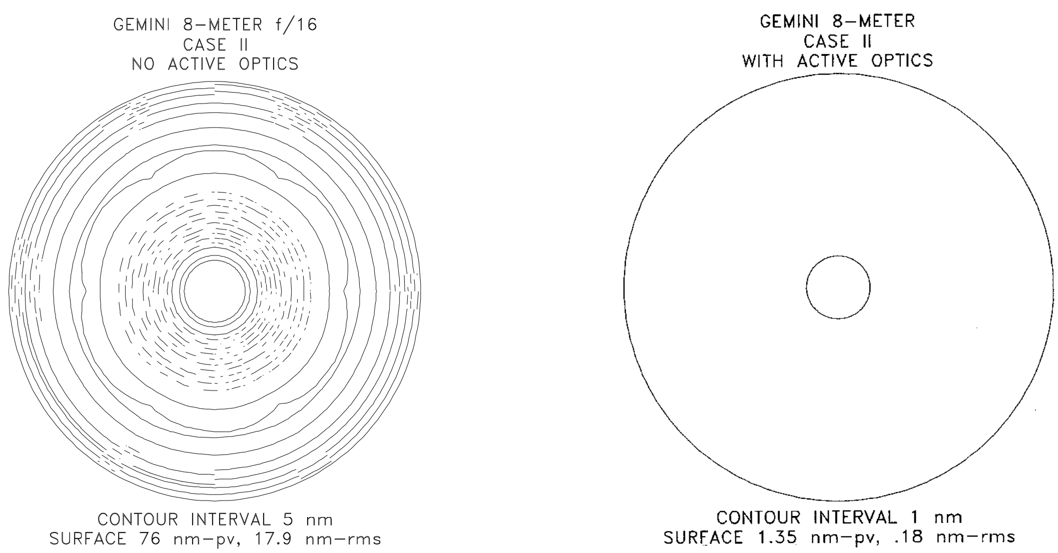

Figure 3. Case II before and after active correction, note the contour interval is 5 times smaller on the right.

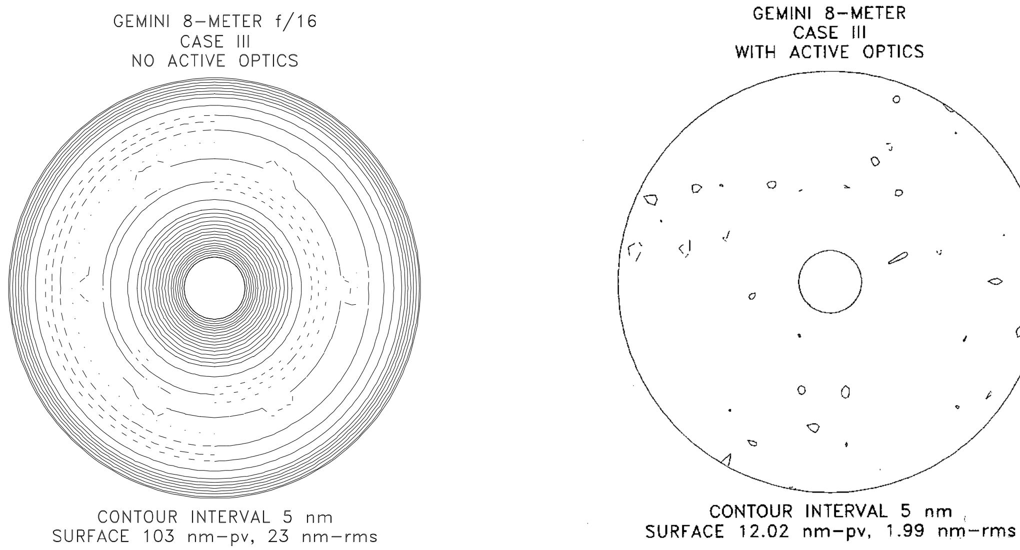

Figure 4. Case III before and after active correction.

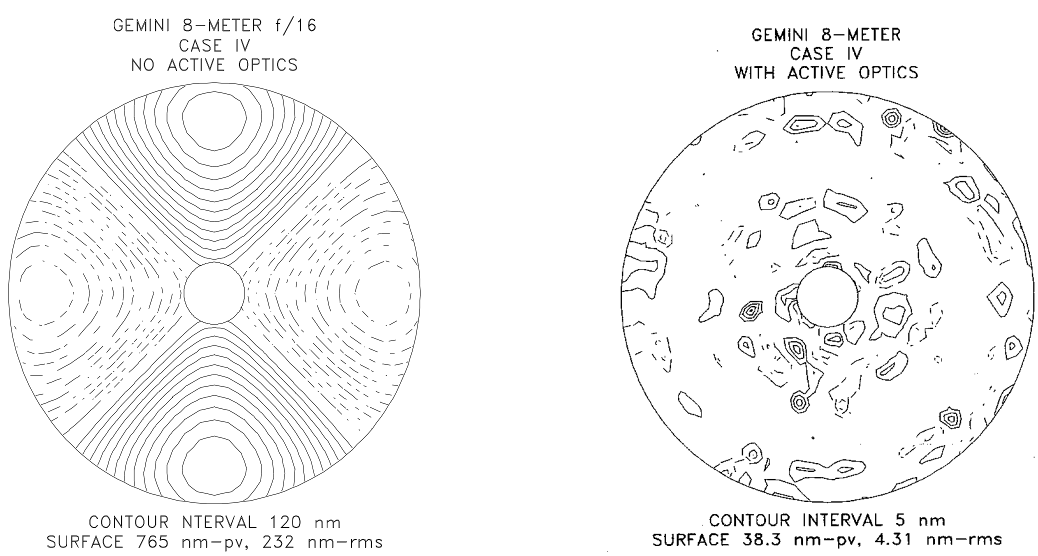

Figure 5. Case IV before and after active correction, note the contour interval is 24 times smaller on the right.

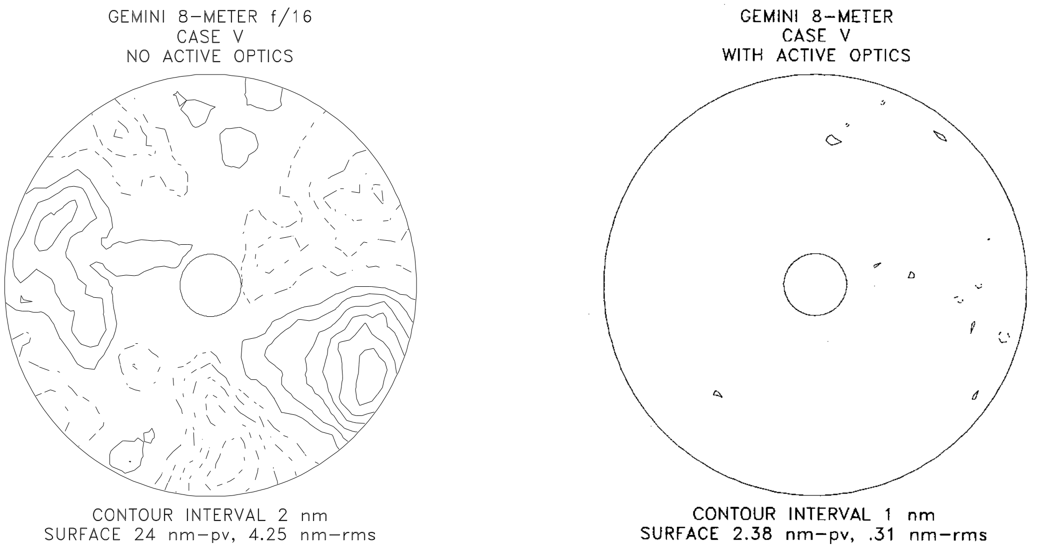

Figure 6. Case V before and after active correction: note the contour interval is 2 times smaller on the right.

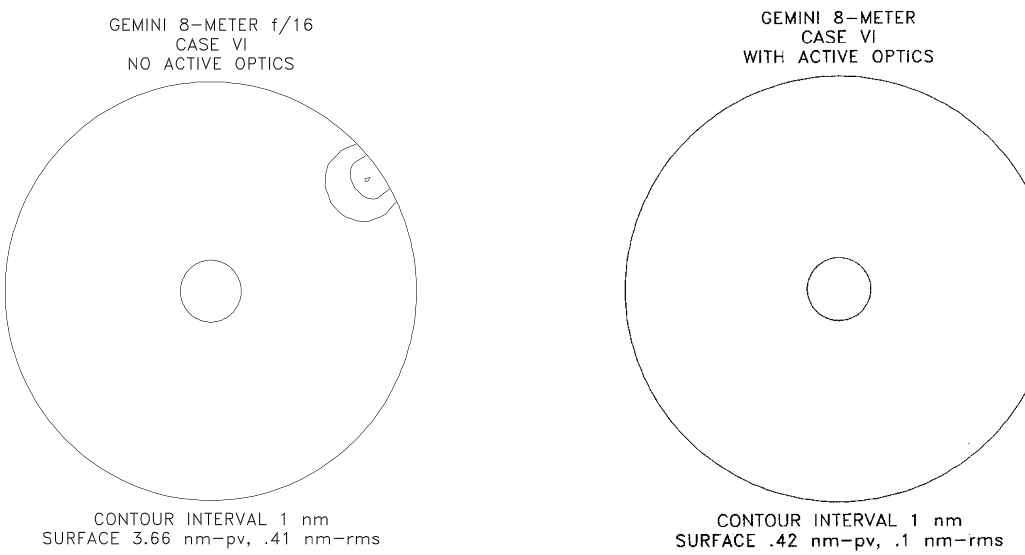

Figure 7. Case VI before and after active correction.

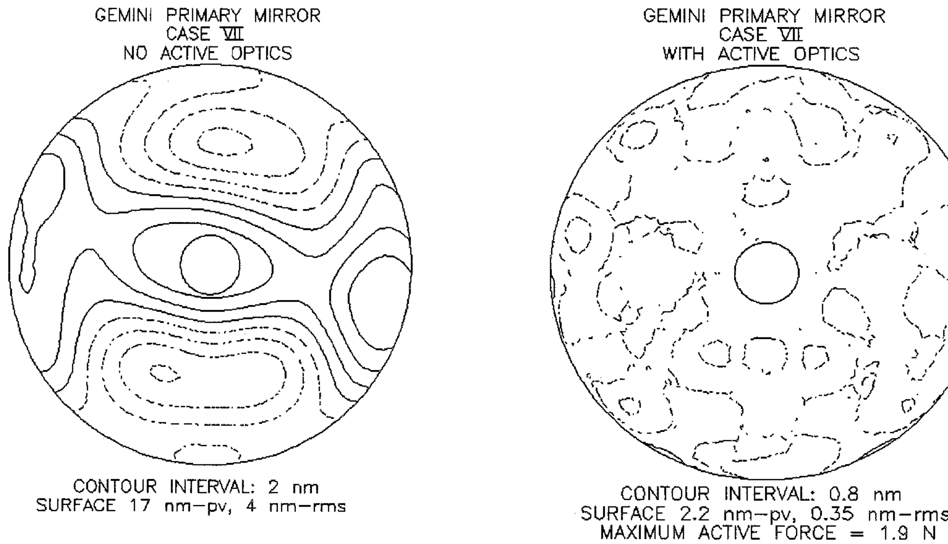

Figure 8 Case VII before and after active correction, note the contour interval is 2 times smaller on the right

4.4 Conclusions

The magnitude of mirror deformation due to thermal expansion is highly dependent on the temperature distribution pattern. For example, case 6, a localized heat input with a one degree C temperature rise produces a 0.4 nm rms surface error. Case 4, however, produced a 575 nm rms deformation, a factor of 1437 larger for the same one degree variation. Because of this, the sensitivity to different temperature distributions will vary.

The design of the primary mirror thermal control equipment determines the most likely temperature distributions. Uniform heating or cooling of the radiation plate behind the mirror will produce axial gradients similar to case 1. Edge effects and nonuniform heating by the surface coating heating system will produce gradients modeled by case 3. These two cases would require four degree gradients each before exceeding the 50% error budget, This is far larger than gradients expected in the mirror during operation of the thermal control equipment.

Due to the low CTE of the ULE primary mirror, the magnitude of thermally induced deformations are low even with large temperature gradients. Most errors of the types analyzed could be several degrees each and still be within the error budget. This is due in part to the smooth shape and slow change rate typical of thermally induced errors, allowing these already small deformations to be further reduced using active optics. Based on the results of this study to date, we predict that the primary mirror thermal distortion error budget, as well as the plate scale error budget, will be met.

Section 5
REFERENCES

1. R. J. S. Greenhalgh, "Design study and tests of a thermal management system for the primary mirrors of the Gemini Telescopes", Gemini Report RPT-O-G0035, 1993.

2. E. Pearson et al, "Planning the national new technology telescope (NNTT): primary optics - tests on a 1.8-m borosilicate glass honeycomb mirror", SPIE Proc. Vol. 628, pp. 91-101, 1986.

3. E. Pearson, L. Stepp, "Response of large optical mirrors to thermal distributions", SPIE Vol 748 Structural Mechanics of Optical Systems II, 1987.

4. I. Mikami, "Hexes pattern optimization method in ULE primary mirror blank", Subaru Telescope technical report no. 19, October, 1992.

5. J. Oschmann, "Gemini system error budget plan", Gemini Memorandum, January, 1992.

6. I-DEAS VI 1990, Structural Dynamics Research Corporation, 2000 Eastman Dr., Milford, OH 45150

7. Code V version 7.53A September, 1993, Optical Research Associates, 550 N Roesmead Bvd. Pasadena, CA 91107

8. M. Cho and R. Price, "Theoretical active optics performances of the Gemini 8-m primary mirror", Gemini Report RPT-O-G0032, 1993